Relationships between Gravity Waves Observed at Earth's Surface and in the Stratosphere over the Continental United States

Catherine D. de Groot-Hedlin[1], Michael A.H. Hedlin[1], Lars Hoffmann[2], M. Joan Alexander[3] and Claudia C. Stephan[4]

[1] Laboratory for Atmospheric Acoustics, Institute of Geophysics and Planetary Physics, Scripps Institution of Oceanography, University of California, San Diego

[2] Jülich Supercomputing Centre, Forschungszentrum Jülich, Jülich, Germany

[3] NorthWest Research Associates, Inc., CoRA Office, Boulder, Colorado

[4] National Centre for Atmospheric Science - Climate, Department of Meteorology, University of Reading, Reading, UK

corresponding author: Catherine de Groot-Hedlin

Key Points:

1) A gravity wave hotspot is detected on the Earth's surface west of the Great Lakes using the USArray Transportable Array barometric network.

2) Gravity wave occurrence rates on the ground exhibit the same broad spatial and temporal patterns as observed at stratospheric altitudes.

3) Evidence suggests that convective activity is the dominant source of gravity waves both at the ground and in the stratosphere.

Abstract

Observations of tropospheric gravity waves made by the new and extensive USArray Transportable Array (TA) barometric network located in the central and eastern United States and of stratospheric gravity waves made by the Atmospheric InfraRed Sounder (AIRS) are compared over a 5-year time span from 2010 through 2014. Gravity wave detections in the period band from 2-6 hours made at the Earth's surface during the thunderstorm season from May through August each year exhibit the same broad spatial and temporal patterns as observed at stratospheric altitudes. At both levels, the occurrence frequency of gravity waves is higher at night than during the day and is highest to the west of the Great Lakes. Statistically significant correlations between the variance of the pressure at the TA, which is a proxy for gravity waves at ground level, with 8.1 μm brightness temperature measurements from AIRS and rain radar precipitation data, which are both proxies for convective activity, indicate that gravity waves observed at the TA are related to convective sources. There is little, if any, time lag between the two. Correlations between gravity waves in the stratosphere and at ground level are weaker, possibly due to the AIRS observational filter effect, but are still statistically significant at nighttime. We conclude that convective activity to the west of the Great Lakes is the dominant source of gravity waves both at ground level and within the stratosphere.

1. Introduction:

Atmospheric gravity waves (AGWs) are a significant driver of global-scale atmospheric circulation and substantially impact weather and climate. They commonly originate in the troposphere, where they are generated by a variety of sources including convective storm systems. Many observational studies have shown the close correspondence of gravity waves with deep convective clouds. Reports of gravity waves observed in surface pressure observations date back to the 1940s and 50s (Brunk 1949; Tepper 1954), but research on these waves and their interactions with convective storms languished until a revival in the 1970s (Bosart and Cussen 1973; Eom 1975; Ucellini 1975). Gravity waves in the stratosphere have been tied to convective storms in early case studies (e.g. Larsen et al. 1982; Pfister et al. 1986; Alexander and Pfister 1995) and more recently in climatological studies with satellite observations from the Atmospheric Infrared Sounder instrument (Hoffmann and Alexander 2010; Gong et al. 2012; Choi et al. 2012; Hoffmann et al. 2013; Tsuchiya et al. 2016; Sato et al. 2016). Gravity waves near the surface can initiate or intensify convective storms (e.g. Stobie et al. 1983; Mapes 1993), and stratospheric gravity waves can influence general circulation, particularly in the tropics and summer hemisphere (e.g. Alexander and Rosenlof 1996; Scaife et al. 2000).

AIRS (Atmospheric Infrared Sounder) is a nadir sounder, sensitive to gravity waves with long vertical wavelengths and short horizontal wavelengths. Nadir sounders provide good horizontal resolution of long vertical wavelength gravity waves, which can cause significant wave drag and carry large momentum flux (Eckermann et al. 2006; Wu et al. 2006; Alexander and Barnet 2007; Preusse et al. 2008). In addition to the climatological studies mentioned above, AIRS data have been applied to case studies of convective

gravity waves related to deep convection, storms, and hurricanes (Grimsdell et al., 2010; Choi et al., 2012; Yue et al. 2014; Stephan and Alexander, 2015). Many observational studies have shown the close correspondence of gravity waves with deep convective clouds. The climatology study of Hoffmann and Alexander (2010) demonstrated that gravity wave occurrence in North America is closely associated with regions of thunderstorm activity. The most active region in North America is located over the Great Plains to the west of the Great Lakes. Most of these gravity waves are associated with deep convection (Hoffmann and Alexander, 2010). Convective gravity waves are most commonly observed by AIRS during local night during the thunderstorm season from May to August.

Although there has been significant progress in observing gravity waves in the middle atmosphere using space-based sensors, it is unclear whether or how gravity waves observed at the Earth's surface are generally related to those observed in the stratosphere. Barometric observations have been made at the Earth's surface since the early 1600's but instrumentation has been variable in quality and the geographic distribution of sensors has been uneven. A new network of barometers has been recently deployed in the United States that addresses many of these shortcomings and gives us an opportunity to use barometric data to further our understanding of how gravity waves in the troposphere relate to those observed in the stratosphere. The network, known as the USArray Transportable Array (TA), comprises 400 identical sensors deployed in a nearly evenly spaced Cartesian grid and is described in the next section. The network has previously been used to study gravity waves that originated near a severe tornadic storm system in the southern US (de Groot-Hedlin et al., 2014). In a case study, Stephan et al. (2016) linked TA surface pressure oscillations and gravity waves observed in the stratosphere to a common precipitating storm source using radar observations and the idealized gravity wave-resolving method of Stephan and Alexander (2015).

In this study, we examine links between surface waves and stratospheric waves more generally. We apply a gravity wave detection method to data recorded by the TA network to compile statistics on gravity wave occurrence and wave properties at ground level for comparison with corresponding observations of gravity waves in the stratosphere made by the AIRS instrument. The study area spans the eastern half of the continental United States and includes observations made over a 5-year timespan from the beginning of 2010 to the end of 2014. This study addresses how gravity wave occurrence varies geographically, diurnally and seasonally across this region, with a particular focus on the thunderstorm seasons each year. In addition to the large-scale analysis, data recorded during the thunderstorm season in 2011 from the hotspot located to the west of the Great Lakes are examined in greater detail to determine whether there is any correlation from day to day between the rate of occurrence of gravity waves on the ground, deep convection events, the background winds, and the occurrence of gravity waves in the stratosphere.

The paper is organized as follows. The datasets are described in Section 2. Section 3 outlines a method for detecting gravity waves using TA data, and presents the occurrence rate at the Earth's surface over a 5 year period from 2010-2014. In section 4, observations

of gravity waves and deep convection in the stratosphere made by the AIRS instrument are described. We discuss the spatial and temporal correlation of gravity waves in the stratosphere and Earth's surface in section 5. A discussion and conclusions are presented in section 6.

2. Data:

2.1 Pressure data from the USArray Transportable Array

The USArray Transportable Array (TA) originated as a broadband seismic experiment on the west coast of the continental United States in 2004 (Busby et al., 2006). By late 2007 the network included approximately 400 stations that were deployed in a Cartesian grid with sites located every 70 km along north-south and east-west lines across a region covering approximately 2,000,000 km^2. Each station was deployed for two years, after which the equipment was transferred from the western edge to a new location at the eastern edge of the network. In this manner, the network gradually moved east across the continental US, reaching the Atlantic coast in 2013. The network was largely removed from the continental US by late 2015 with most stations being re-deployed in a less dense (85 km spaced) configuration in Alaska and Canada's Yukon territory.

Beginning in the second half of 2009, atmospheric packages were added to each new station in the network. This package included a micro-electromechanical system (MEMS) pressure sensor (sensitive from DC to 100 s), a Setra 278 (DC to 1 Hz) and a Hyperion high-frequency infrasound microphone (sensitive from 200 s to above the Nyquist frequency). A map of the upgraded stations, shown in Figure 1, shows the change in the location of the network over time since the upgrade began. In total, over 1,000 sites were occupied in the continental US. Data from all stations are digitized at 1 and 40 sps and then telemetered in near-realtime to the Array Network Facility (ANF) at UC San Diego for preliminary processing before being forwarded to the Data Management Center (DMC) in Seattle, WA where they are archived and made available to the general public. The installation of MEMS sensors began several months before the other sensors. Since MEMS data are available at more sites than the other sensors, and have a sufficiently broad frequency range, they were used for this study. These data are digitized at 1 Hz.

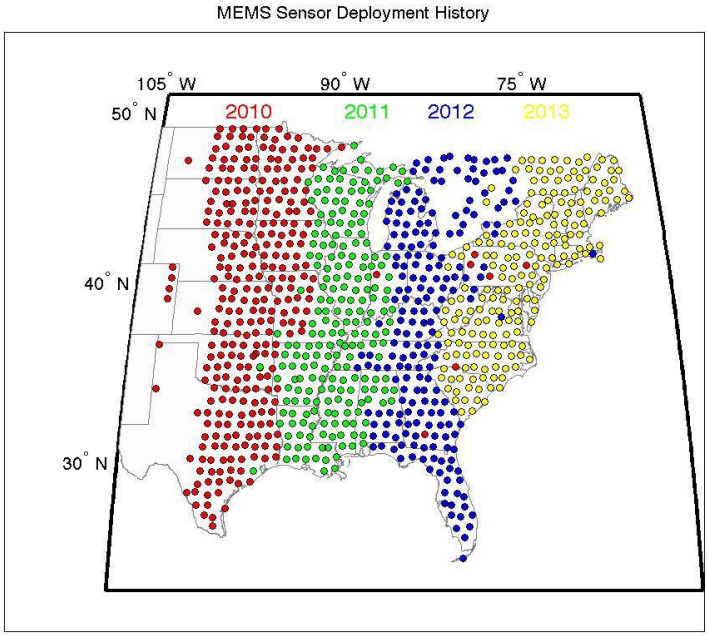

Figure 1. Deployment of stations in the TA that include MEMS sensors. Stations are color coded by the year they began operating. Each station was left in place for two years before being moved from the west to the leading (eastern) edge of the network.

2.2 Satellite data

The AIRS sensor (Aumann et al., 2003; Chahine et al., 2006) is located aboard NASA's Aqua satellite, which was launched in a nearly polar, low earth orbit in May 2002. Aqua achieves nearly global coverage during 14.4 daily orbits. The orbit is sun-synchronous, with Equator crossings at 01:30 LT (descending orbit nodes) and 13:30 LT (ascending orbit nodes). AIRS measures infrared radiance spectra from the Earth's atmosphere in the nadir and sub-limb geometry.

Information on gravity wave activity is inferred from AIRS radiance measurements using the approach of Hoffmann and Alexander (2010) and Hoffmann et al. (2013, 2014). The spectral mean brightness temperatures (BTs) are analyzed in the 4.3 μm CO_2 fundamental band, which gets optically thick in the mid-stratosphere at about 30-40 km altitude. There are three main contributions to the observed BT: (i) gravity wave signals, (ii) background signals varying on large scales, and (iii) measurement noise. The detrending procedure of Alexander and Barnet (2007) is used to remove the background signals associated with large-scale temperature gradients and limb brightening. Given the footprint size of the satellite scans, the lower horizontal wavelength limit of the gravity wave observations is about 30 km. The 4.3 μm BT variances shown in this paper have been corrected for noise, by subtracting noise variances scaled to scene temperature.

As an example, Figure 2 shows AIRS observations of stratospheric gravity waves over the North American Great Plains on 27 June 2011. Measurements are shown for the descending parts of the satellite orbits, which are nighttime measurements (01:30 local time). The 4.3 μm BT perturbation map reveals significant convective wave activity to the southwest of the Great Lakes. The AIRS observations show semi-circular wave fronts/patterns to the east of the convective sources. Wave patterns to the west of the convective sources are not observed by AIRS. The east-west difference is predominantly due to the prevailing westerly background winds, causing Doppler-shifting towards long vertical wavelengths in the east and short vertical wavelengths in the west. Gravity waves with long vertical wavelengths are more clearly visible to AIRS due to the nadir observation geometry. Short-scale waves with horizontal wavelengths of less than about 100 km are found close to the convective sources whereas larger-scale waves are found at greater distances, having propagated further from the convective sources. This is consistent with linear wave theory and the horizontal wavelength dependence of horizontal group velocity. Propagation of the convective sources, and filtering by the background wind, which occurs when a wave approaches a level where the wave phase speed equals the wind speed, may additionally contribute to the observed east-west asymmetry.

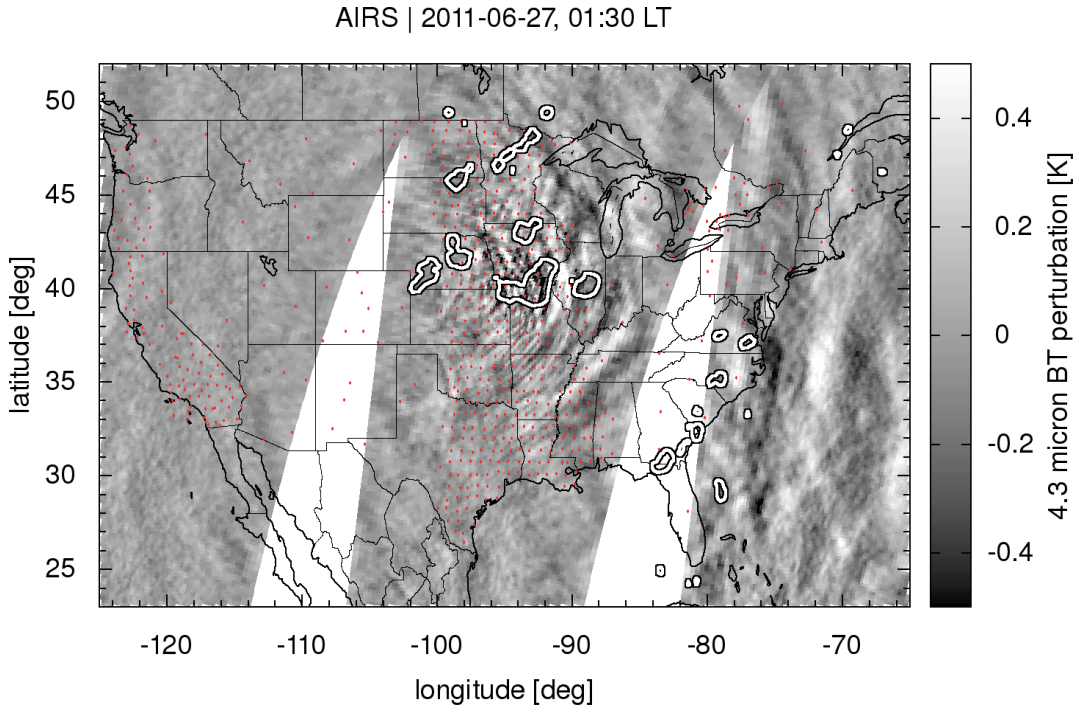

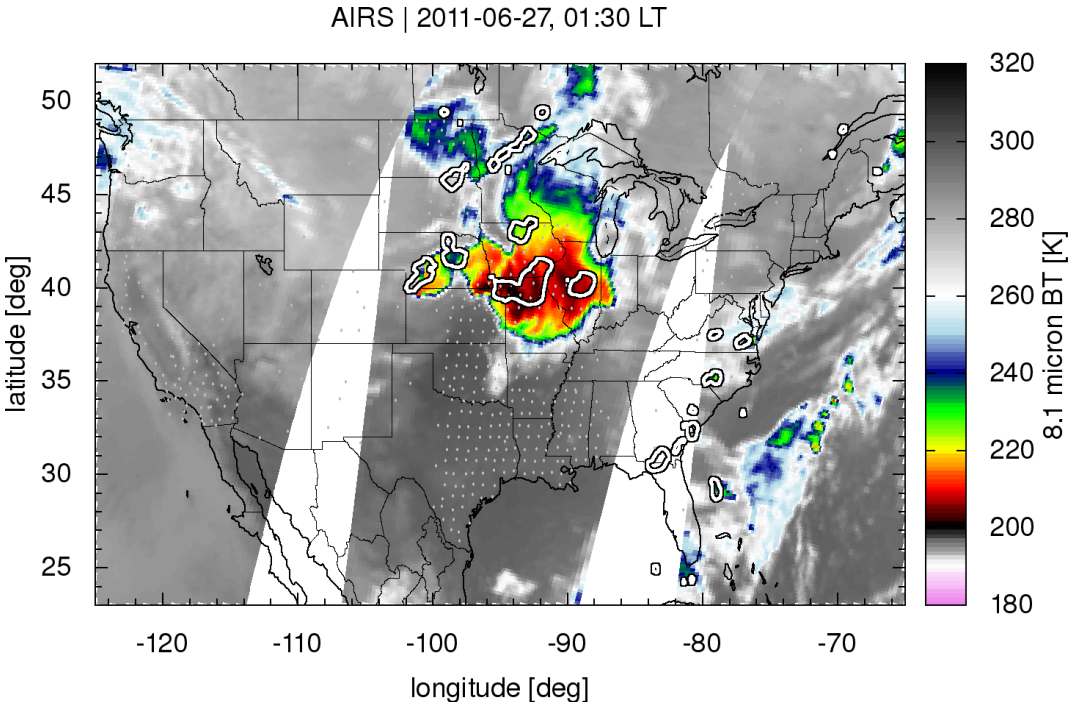

Figure 2. The upper and lower panels show BT perturbations in the 4.3 μm spectral region and BTs in the 8.1 μm spectral region, respectively. These images were taken from AIRS radiance measurements on June 27, 2011 at 01:30 local time during the descending orbit. Contour lines in both panels show 6 mm/hr maximum precipitation rates for 07:00 UTC. The small dots show the TA station locations on that date.

2.3 Precipitation data

The National Centers for Environmental Prediction/Environmental Modeling Center's (NCEP/EMC) gridded Stage IV precipitation data is a mosaic produced from radar observations. It is based on the multi-sensor hourly Stage III analysis produced by the 12 River Forecast Centers in the continental U.S. After a manual quality control performed at the River Forecast Centers it is made into a national product. The dataset is available from 1 Jan 2002 onwards on a polar-stereographic grid with a resolution of 4.7625 km at 60° N. For this study the average and maximum precipitation rate are computed on a coarse grid, where each coarse grid box is formed of 7x7 Stage IV grid cells.

3. Gravity wave observations at Earth's surface

3.1 Detection method for gravity waves

The large region covered by the TA network allows for the detection of long wavelength pressure perturbations and observation of how the properties of these signals change with time and location. Data from this network were used by de Groot-Hedlin et al., (2014) to track the motion of gravity waves generated near a convective storm system across the

US. The study showed that, given the geometry of the TA and the amplitude spectrum of the observed gravity waves, signals with periods of several hours could be followed. Tepper (1954) found that most surface pressure waves were are periods under 6 hrs. Other studies (Eom, 1975; Ucellini, 1975; Stobie et al., 1983) also observed waves in the 2-6 hr period range. Consequently, a period band from 2-6 hours was chosen for this study. Figure 3 shows 2-6 hour band-passed recordings made on June 27, 2011 by MEMS sensors located between longitude 93 to 94° W, the same day that the AIRS instrument detected a large signal in the stratosphere (Figure 2). Large signals in the 2-6 hr passband are observed near 38-44°N between 01:00 and 13:00 UT, and are seen to be travelling to the south and north at later times. The signals are coherent between stations.

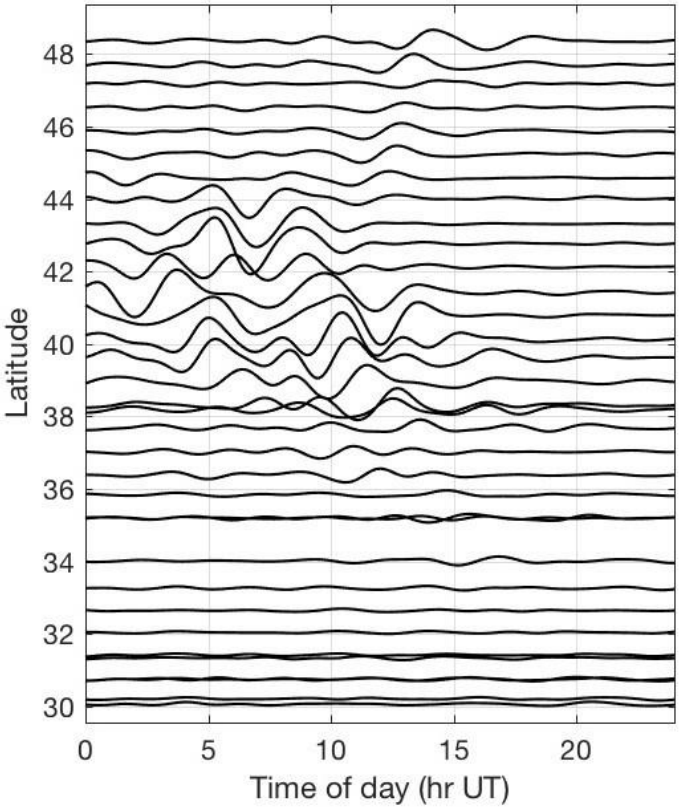

Figure 3. Record section from June 27, 2011 using stations located in a north-south column of the TA between longitudes 93° W and 94° W. Each horizontal line is a recording from one station, bandpassed from 2-6 hours. The scale is 400 Pa per degree latitude. Waves with amplitudes ~100Pa are observed to propagate both northward and southward from a central region near 42N.

Figure 4 shows maps of the band-passed pressure recordings across a large region west of the Great Lakes at two time points, separated by 30 minutes. These times - 06:30 UT and 07:00 UT are close to 01:30 LT that day; the time of the image from the AIRS instrument (Figure 2). As shown, signal wavelengths are greater than the inter-station spacing and

are coherent between stations, making them amenable to array processing to obtain estimates of their arrival time at any point in the network, phase velocity, propagation direction and amplitude. Signal motion is apparent from these two time points; in this time range, the dominant direction of motion is toward the southeast.

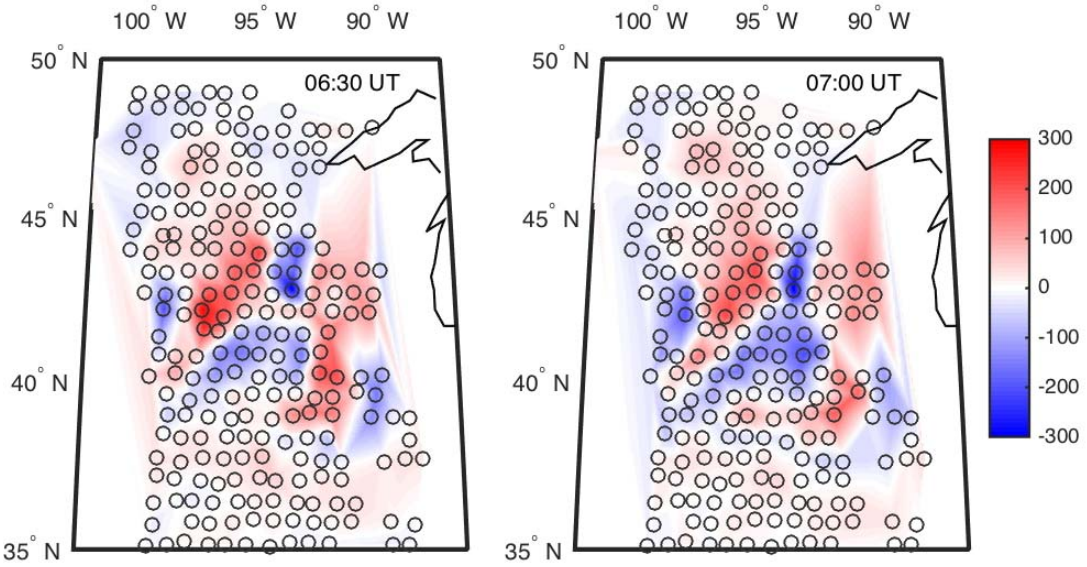

Figure 4. Maps of the pressure variations (in Pa) in the 2-6 hr band at two times (06:30 and 07:00 UT) on June 27, 2011. The band-passed pressure measurements are spatially interpolated between stations, shown by the open circles.

An algorithm to detect weak, long-wavelength signals that are detectable over only a subset of sensors within a broader network, described in de Groot-Hedlin et al. (2014), is applied here to detect propagating gravity waves. First, the Delaunay triangulation (Lee and Schachter, 1980) is used to discretize the network into a large number of non-overlapping, adjacent arrays, each comprising three adjacent stations (called triads). For each triad, an array analysis is performed over a series of time windows of 16 hours duration, with two-hour time-steps between windows, which gives 14 hours of overlap between time windows. This temporal spacing allows for examination of diurnal variations in the gravity wave occurrence rates. Briefly, the array analysis consists of cross-correlating the band-passed waveforms for each of the three station pairs within each triad to find the time delays due to propagation between stations. In most cases the computed time delays around a triad are inconsistent with a single coherent signal (Cansi, 1995), and null values are retained for the signal characteristics. However, if the time delays are consistent (i.e., the signal is assumed to be consistent with a planar wavefront crossing the array), a tau-p method (Havskov and Ottemöller, 2010) is applied to the time delays to derive the signal's propagation direction and phase velocity. These characteristics are used to time shift the individual waveforms measured at each sensor within the triad to bring the common signal into best alignment. The sum of these waveforms is referred to as a beam, and the process is called beamforming. The peak

amplitude and corresponding arrival time of the beamformed signal are taken as additional signal characteristics, along with the phase velocity and azimuth. This analysis is repeated for each time window, for each triad within the network.

The results of these array analyses are shown in Figure 5a, for coherent signals with peak amplitudes occurring between 03:30-09:30 UT, June 27, 2011, which is local nighttime. The pressures at the Earth's surface in this time range were shown in Figure 4. Circles, color-coded by the amplitude of the beamformed signal, show where coherent gravity waves are detected. The arrows connected to the circles show the direction of wave propagation. In this example, the wavefront moves predominantly to the southeast. The phase velocities of the signals are not shown, but lie in the range from 12-96 m/s, consistent with atmospheric gravity wave velocities.

The calculation of the occurrence frequency of gravity waves for any given region is complicated by the fact that the TA moved significantly to the east over the study period. To quantify the detection rate, the map area covered by the TA is pixelated, with each pixel extending from 0.75^{o} north-south and 1^{o} in the east-west direction, so that they are approximately square. The occurrence rate for any given pixel is defined as the number of time periods in which coherent gravity waves are detected within that pixel, divided by the number of time periods over which any triads spanned at least part of that pixel. Figure 5b shows the regions in which long wavelength signals were detected, as shown in Figure 5a, and the area in which the TA resides. For any given time window, a pixel is 'active' if one or more triads that lie at least partially within it detect a gravity wave. The active pixels are shown in dark red in Figure 5b. The light green pixels show areas in which the TA is deployed, but no gravity waves are detected for this time period.

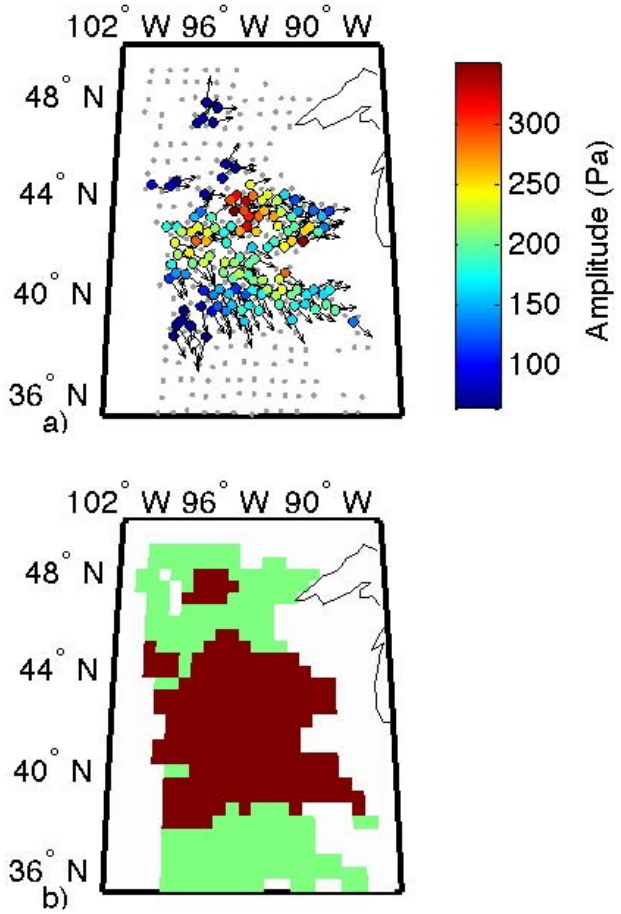

Figure 5. a) Signal pressure amplitudes and direction of motion detected at the TA within the time period from 03:30-09:30 UT on June 27, 2011, coinciding with local nighttime. Each circle represents a coherent gravity wave detection at a single triad, color-coded by the amplitude of the beamformed signal. The arrows show the direction of propagation. Station locations are indicated by gray dots. b) Green pixels show areas where the TA was deployed but gravity waves were not detected for this time period. Red pixels show areas where detections were made.

This method detects any coherent long wavelength signal crossing over a subset of the array. In practice, not all detections are considered further for this analysis because the goal here is to focus on gravity waves generated by convective sources. A separate analysis showed that most of the smallest signals detected, below 60 Pa, have a seasonal dependence that clearly distinguished them from the larger signals. The arrival time of these low amplitude signals, which are observed across the study area, is linked to sunrise and sunset indicating a different origin. Although the lower threshold of 60 Pa removes some signals associated with convective activity, as can be seen in Figure 3, this cutoff primarily serves to remove signals caused by another source mechanism. We also apply a mask to areas where the rainfall, as defined by the NCEP/EMC precipitation data, is

over 2 mm/hr within 30 km of a TA site. After application of the mask, the remaining 2-6 hr period signals are identified as AGW. This algorithm is used to create a catalog of detections that are used to assess the occurrence rate of gravity waves in the 2-6 hr frequency band observed at Earth's surface, which are then compared with measurements made by the AIRS instrument. The catalog also includes the wave properties of each detected wave.

3.2 Gravity wave occurrence frequencies at the Earth's surface

Past studies (including Hoffmann and Alexander, 2010) have revealed a high level of gravity wave activity at local night during the thunderstorm season from May through August (MJJA) in the area to the west of the Great Lakes. The TA crossed this region from 2010-2012 and continued to the east coast by 2014. This study focuses on two time segments of the year during 5-year period; the thunderstorm season (MJJA) and the remainder of the year (September 1 through the end of April, known here as SONDJFMA). Figure 6 compares the occurrence rate of AGWs over the entire day during MJJA with those made during SONDJFMA. The area of gravity wave activity is strongly concentrated in a region to the west of the Great Lakes during the thunderstorm season, with a 30% probability of detecting a gravity wave at least once a day during these months. Coherent gravity waves are detected over a broader region during the remainder of the year, with a peak occurrence rate of 16%.

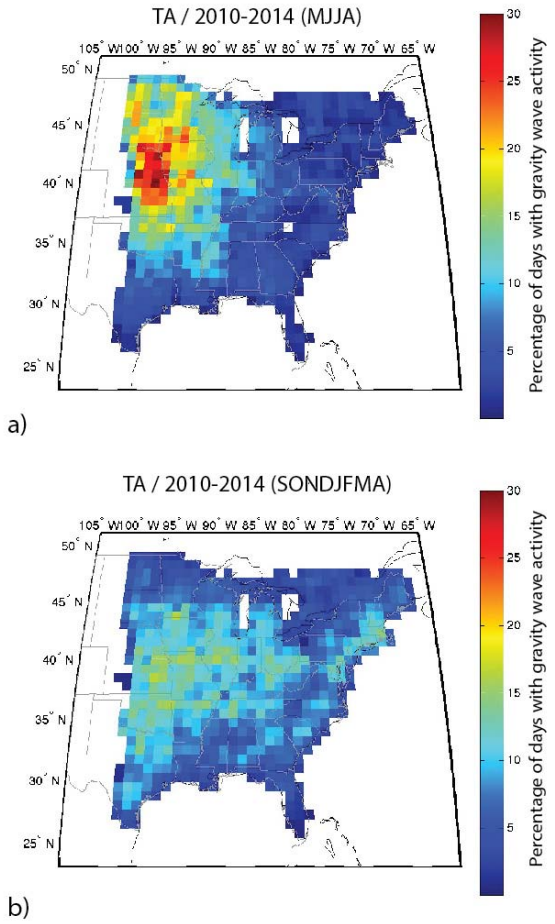

Figure 6. Occurrence rate of gravity waves in the 2-6 hr frequency band observed at Earth's surface for a) the 4 months from May through August and b) the 8 months from September through April during the 5-year timespan from 2010-2014.

The occurrence rates for the thunderstorm season were further broken down into two six-hour time periods each day - from 03:30-09:30 UT and 15:30 to 21:30 UT - as shown in Figure 7. The first time period spans 01:30 LT (i.e. local night) and is comparable to observations made by the AIRS instrument during the descending orbit. The second period is local daytime and includes the 13:30 AIRS overpass. As shown, the occurrence rates differ between the two time periods. Similar to AIRS, gravity waves are detected at ground-level more frequently at night than during the day, and most detections are made to the west of the Great Lakes. The local night time occurrence rate rises to 17.3% at 38-44 ^{o}N and 94-99 ^{o}W. During the local daytime hours, the occurrence frequency is much less concentrated as shown in Fig. 7b, and reaches a maximum of 8.9%. The percent of time that rainfall exceeds 2 mm/hr during these time intervals is also shown in this figure.

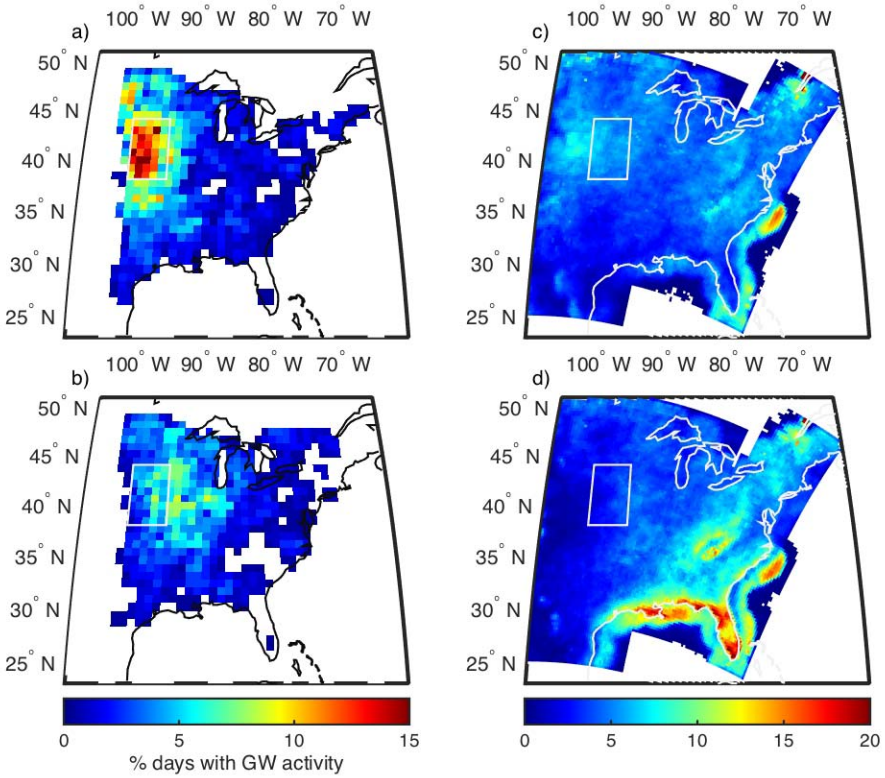

Figure 7. Occurrence rate of gravity waves in the 2-6 hr frequency band observed at the Earth's surface during thunderstorm season (May-Aug) during a) local night (03:30-09:30 UT) and b) local day (15:30-21:30 UT). c) and d) show the percentage of time rainfall exceeded 2 mm/hr during the same time intervals. Note that the color scale used on the left is different than in Figure 6. The area outlined in white in each panel is where surface gravity wave activity is greatest, from 38-44 ^{o}N and 94-99 ^{o}W.

As discussed above, array processing at each triad also gives information on the speed and direction of gravity wave signals and how these quantities vary across the study area. The histograms in Figure 8 show the direction of motion for AGW detections made in May to August from 2010 through 2014 during local night. For clarity, the detections are grouped over larger areas than in the previous plots; each angle histogram covers a nearly square region of 3^{o} north-south by 3.9^{o} east-west. The angle histograms are polar plots that show the distribution of AGW propagation directions, in angular bins of 20^{o}. The length of each bin reflects the number of AGWs with a propagation direction in that angular range. The longest spoke of each histogram indicates the dominant AGW direction. The color coding shows the mean AGW amplitude for each bin. As shown, most of the detected AGW propagate to the ESE and their amplitudes are greatest to the west of the Great Lakes, where they are most common. Their eastward motion may be due to the fact that rainfall is heaviest just to the west of the AGW hotspot.

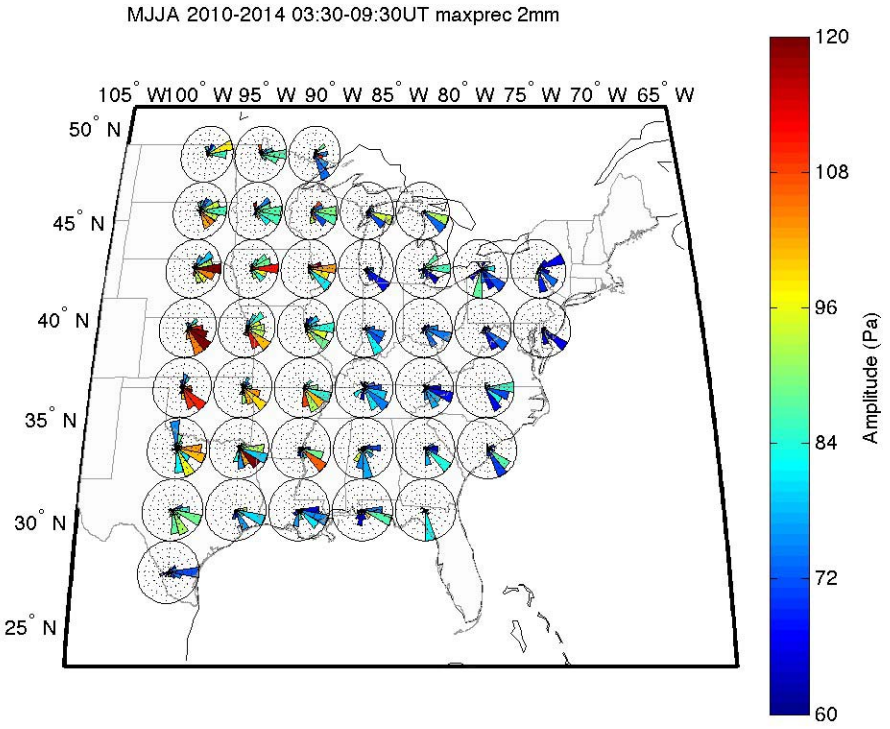

Figure 8. Angle histograms showing direction of propagation and amplitude of coherent waves detected during the thunderstorm seasons from 2010-2014. All detections were made during the local night (from 03:30-09:30 UT). The largest waves are seen to the west of the Great Lakes. Most signals propagate to the ESE.

4. Observations of gravity waves and deep convection in the stratosphere

Figure 9 shows AIRS occurrence frequencies of stratospheric gravity waves and convective events over the North American Great Plains during May to August for the years 2010 to 2014. The occurrence frequencies were calculated following the approach outlined by Hoffmann and Alexander (2010) and Hoffmann et al. (2013). Gravity wave events are identified if the local variance of the 4.3 μm BT perturbations within a radius of 100 km around each footprint exceeds a threshold that is significantly larger than the measurement noise. Similarly, convective events are identified if the 8.1 μm BT measurement for a footprint drops below a threshold that is indicative for the presence of cold cloud tops related to deep convection in the instrument's field of view. Following Hoffmann et al. (2013), we applied thresholds that depend on latitude, month, and time of day. Hoffmann and Alexander (2010) used a fixed-threshold approach for their study, but we found that the variable-threshold approach used by Hoffmann et al. (2013) generally copes better with varying measurement noise of the AIRS instrument. Occurrence frequencies are calculated from event / non-event counts for individual satellite footprints based on an 0.5° x 0.5° longitude-latitude grid. The analysis is conducted separately for nighttime (01:30 LT, descending parts of satellite orbits) and daytime (13:30 LT, ascending parts of satellite orbits).

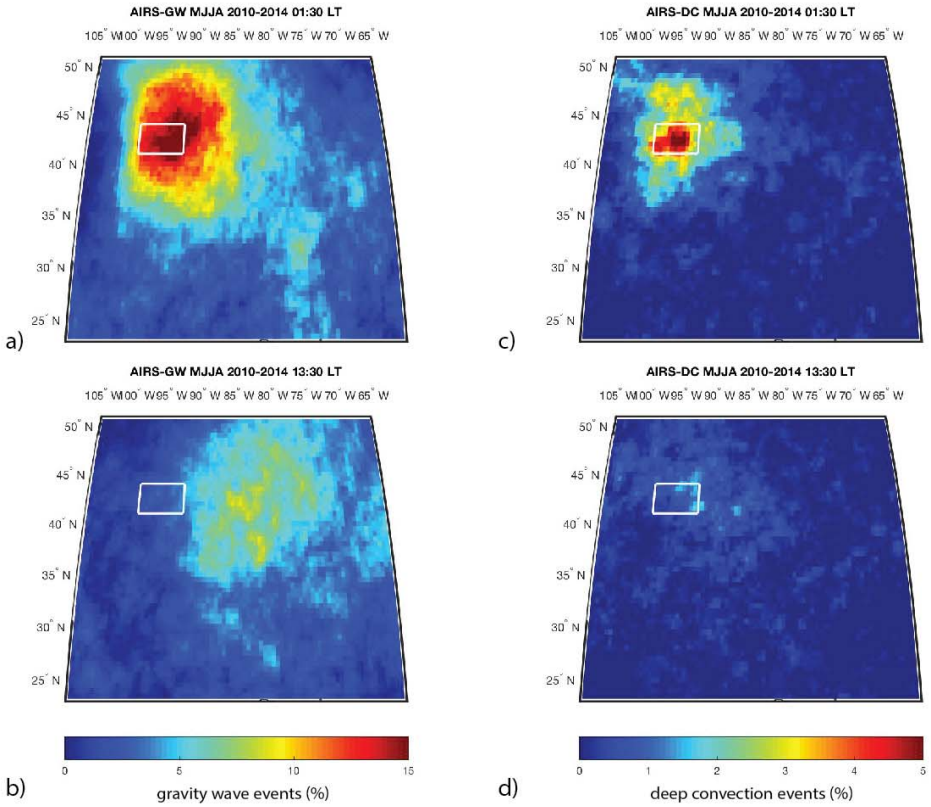

Figure 9. In the left column the occurrence frequency of gravity waves in the stratosphere is shown over the entire study area from observations made by the AIRS instrument during May through August from 2010 through 2014. Results from descending orbits at 01:30 LT and ascending orbits at 13:30 LT are shown in (a) and (b) respectively. The panels in the column on the right show the occurrence frequency of deep convection events for the descending and ascending orbits (c and d respectively). The pixels in these images are 0.5° on a side. The area outlined in white in each panel is where convective activity at nighttime is greatest, from 41-44°N and 92-98°W.

The patterns of gravity wave and convective activity found in the AIRS data for the years 2010-2014 in Fig. 9 are quite similar to those reported by Hoffmann and Alexander (2010) for the years 2003-2008. In the nighttime measurements we found significantly increased wave activity (occurrence frequencies of 5-15%) at 35-50°N and 86-98°W, with the maximum of wave activity being found at 40-45°N and 92-96°W. This increase in wave activity is associated with increased convective activity (occurrence frequencies of 2-5%) at 35-50°N and 86-102°W, with a local maximum at 41-44°N and 92-98°W. Hoffmann and Alexander (2010) explained the eastward shift of the gravity wave maximum with respect to the convective maximum based on predominant eastward propagation (cf. Figure 2) and better observability of eastward propagating waves by AIRS. At daytime, the hotspot of convective wave activity over the North American Great Plains is still visible, but occurrence frequencies of both convection and gravity

458 waves are much lower than at nighttime. This is attributed to the diurnal cycle of
459 convection, which relates to mesoscale convective systems intensifying over the Great
460 Plains at night in the summer thunderstorm season [e.g. Carbone and Tuttle, 2008]. We
461 found that convective wave activity outside the thunderstorm season (from September to
462 April) is relatively weak (not shown).
463
464 **5. Joint observations of gravity waves in the stratosphere and Earth's surface**
465
466 The array analysis method used to detect gravity waves at the Earth's surface measures
467 the time rate-of-change of long period pressure signals crossing the TA, while gravity
468 waves in the stratosphere are identified by computing the spatial variation of the BT for a
469 given orbit. It is notable that, using these very different instruments and analysis methods
470 over the five year study period, gravity wave occurrence frequencies at the Earth's
471 surface, shown in Figure 7, show similar spatial and temporal patterns as at stratospheric
472 altitudes, shown in Figure 9. However, the array analysis method described in Section 3
473 does not allow for a direct day-to-day comparison of gravity wave activity at the ground
474 and in the stratosphere. For this, we compute the spatial pressure variations measured by
475 TA barometers at a given time point and compare these to the spatial 4.3 μm BT
476 variances which serve as a proxy for gravity wave activity in the stratosphere. The spatial
477 pressure variances are computed over a given region by mapping the pressure in the 2-6
478 hr band at a given time point, similar to the maps shown in Figure 4. We then computed
479 the pressure variance within that region to obtain a measure of the gravity wave activity
480 at that given time point. The pressure variations are computed hourly. As before, data at
481 any station are masked when the peak precipitation exceeds 2 mm/hr. We also computed
482 the hourly total rainfall within this region.
483
484 Our analysis aims to identify whether gravity waves in the two data sets are likely related
485 to the same convective activity, and the degree of correlation between the rainfall and
486 pressure variances. The regions of interest chosen for this day-to-day comparison of
487 AIRS and TA gravity wave observations, and the rainfall, are to the west of the Great
488 Lakes, from 41-44°N and 92-98°W which captures the zones of most intense gravity and
489 convective wave activity for the AIRS measurements, and from 38-44°N and 94-99°W
490 for the rainfall measurements and the AGW region captured by the TA pressure
491 measurements. The AIRS region is further east than the TA region because we know that
492 waves observed by AIRS in the stratosphere systematically propagate further east from
493 their source, while waves seen at the surface may appear closer to their source. The time
494 interval is from JD 121 to 243, 2011, which includes the thunderstorm season for the year
495 that the TA had the greatest coverage of the region of interest. Figure 10 compares
496 observations from the AIRS sensor and the TA pressure sensors, and the precipitation
497 statistics. Figure 10a shows the minimum BT at 8.1 μm for each pass across the region
498 of interest; low values for these measurements are considered a proxy for convective
499 activity. The European Centre for Medium-Range Weather Forecasts (ECMWF) ERA-
500 Interim reanalysis 6-hourly zonal and meridional winds at an altitude of about 35 km are
501 shown in Figure 10b. Figure 10c shows the noise corrected variance of BT perturbations
502 at 4.3 μm, which is a proxy for gravity wave activity in the stratosphere. In Figures 10a
503 and 10c, the nighttime measurements are shown in red; the daytime values are shown in

green. Figure 10c shows that the four largest gravity wave events during the thunderstorm season in 2011 occurred during local night on JD 169, 171, 178 and 192. Figure 10d shows the total precipitation within the the study area for the TA, computed hourly. Figure 10e shows the pressure variances within this same region. The four dates of greatest activity in the stratosphere are marked in the lowest panel by the green lines.

There is significant agreement between ground and satellite observations, particularly linking convective storm activity to the pressure variance at the Earth's surface. A visual inspection of Figs 10a and 10e indicates that periods of high convective activity, marked by low 8.1 μm BT measurements, are concurrent with periods of high pressure variances measured at the TA. To obtain a quantitative assessment, we compute the Spearman rank-order coefficient r_s and Pearson linear correlation coefficient r. Both coefficients range between -1, indicating a negative correlation and +1, indicating positive correlation, with values near zero indicating that the pairs of variables are uncorrelated. The Spearman rank correlation coefficient, which considers the ranking of the data points rather than their absolute values, is the more robust measure of correlation as it is less sensitive to outliers. Spearman's correlation is sensitive to almost any monotonic correlation in the data, whether linear or not. Tests of the statistic significance exist for the Pearson and Spearman correlation coefficients. More details on these statistical measures can be found in Press et al. (2002).

Comparing the AIRS observations of 8.1 μm BT values to the pressure variance values with no time lag for the 2011 thunderstorm season, we find that r_s for the nighttime passes is -0.63 with a significance value below 10^{-13}, indicating that the nonparametric correlation is highly significant. The Pearson r value is -0.4, indicating a moderate linear correlation. The negative correlation values imply that higher levels of convective activity, as indicated by low 8.1 μm BTs, correlate to higher levels of gravity wave activity near the surface, as expected. The corresponding values for the daytime passes are r_s = -0.39 with a significance of 2.7×10^{-7} and r = -0.2, indicating that correlations are weaker and less linear. These correlation values are for direct temporal correlations, and do not take into account any time lag between gravity waves observed at the Earth's surface and convective storm activity as measured by the AIRS instrument. Because the TA data have a high time sampling rate, we are able to cross-correlate pressure variance values and the AIRS measurements as a function of time. We find that correlation values for nighttime passes peak between zero to one hour after the satellite pass, indicating a very small time-lag between convective activity and the corresponding surface gravity wave activity. The correlation values tend sharply to zero after a two hour time delay. This pattern holds for daytime passes as well, with peak correlation from zero to one hour after the satellite pass, and correlations decreasing after a two hour lag. Comparison of the hourly precipitation with the pressure variances indicates a much lower correlation, with r_s = 0.24, with a significance below 10^{-30} indicating that the correlation is highly significant. The Pearson statistic indicates a poor correlation.

The link between gravity wave activity at the ground and in the stratosphere appears weaker. To make such a comparison first requires consideration of the stratospheric winds (Fig. 10b), because waves are generally only visible to AIRS sensors when those

winds are strong. So we focus on the June-August period. Within that period, a visual inspection of Figs 10c and 10d indicates that three of the days identified as being highly active in the stratosphere (JD 169, 171 and 178 in Figure 10c) are also active on the ground. This is particularly true on JD 178 (June 27 discussed earlier). The fourth highly active day in the AIRS timeseries, JD 192, is not unusually active on the ground. There are several other days earlier and later in the thunderstorm season during which the pressure variances are significantly greater than the background level, but the 4.3 μm BT variance is not significantly enhanced in the AIRS timeseries for these days. The analytic measures of correlation between the 4.3 μm BT variance and the pressure variance measurements on the ground are much higher for nighttime satellite passes than for the day. The Spearman r_s value peaks at 0.47 from zero to one hours after the night-time satellite pass, with significance values of approximately 10^{-7}, indicating significant correlation. The correlations decrease significantly after a two hour time delay. The Pearson r values for zero to 1 hour time delays are approximately 0.55, indicating significant linear correlation. Correlation values for daytime passes are insignificant. We note that these comparisons were made for the entire thunderstorm season, regardless of the strength of the zonal wind; Alexander and Barnet (2007) report that stationary orographic gravity waves are detected by AIRS only when horizontal winds exceed about 40 m/s, which is attributed to the observational filter effect. For travelling waves from convection, this threshold will be lower: we estimate closer to 10 m/s. This wind effect can also be seen by comparing Figs. 10b and 10c.

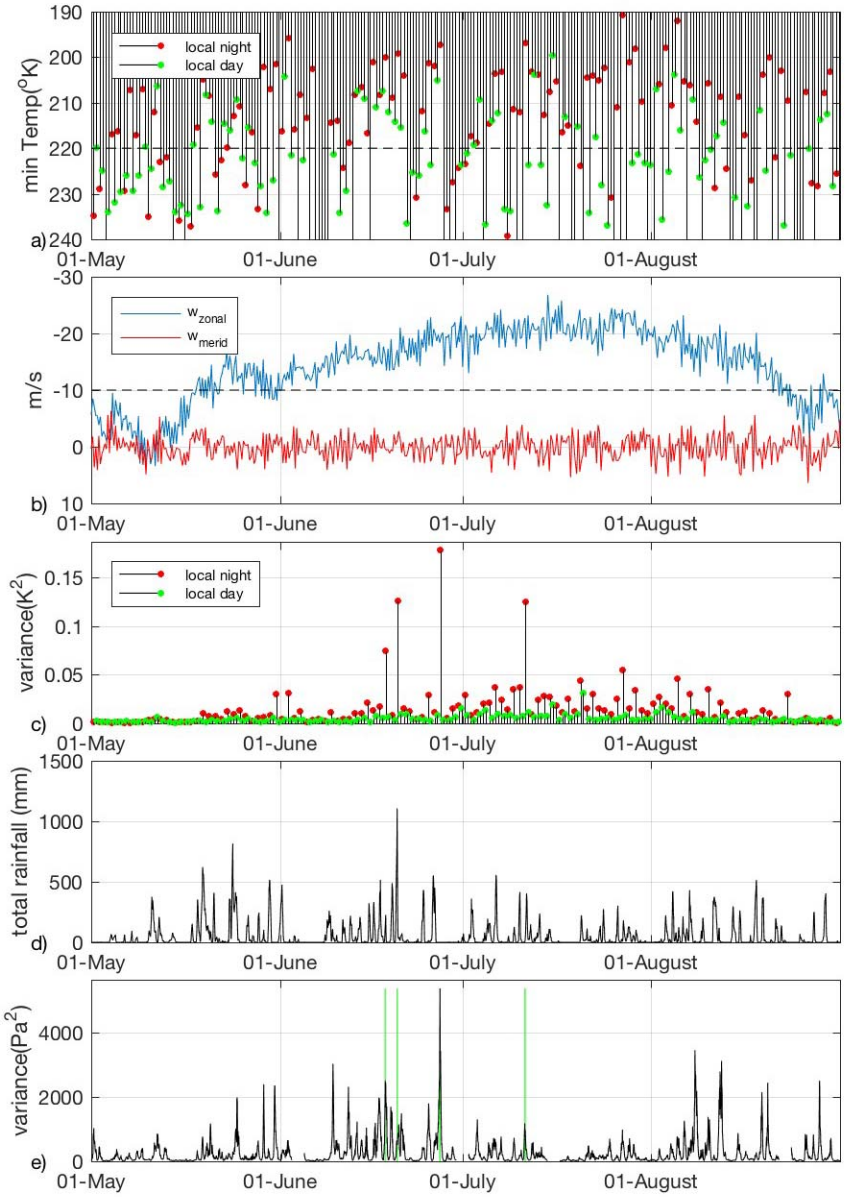

Figure 10. a) The AIRS minimum BT at 8.1 μm, which is a proxy for convective storm activity. Values from the ascending branch (local daytime measurements) are shown in green; red dots indicate values from the descending branch (local night time). A dashed line at 220° K is a typical threshold for detecting deep convection as used in Hoffmann and Alexander (2010); a variable-threshold approach is used here and in Hoffmann et al. (2013). b) ERA-Interim zonal and meridional winds at ~35 km altitude at 6 hour time intervals. The dashed line at 10 m/s marks the stratospheric wind speed below which AIRS detections of gravity waves are not expected . c) The variance of AIRS 4.3 μm BT perturbations, which is a proxy for gravity wave activity in the stratosphere. The values for plots a), b) and c) are taken over the rectangular region from 41-44°N, 92-98°W. d) The total rainfall over the nearby region in which gravity waves are most frequently detected by the TA (38-44°N, 94-99°W) per hour. e) The recorded pressure variance in the 2-6 hr band made by TA sensors in this region. Pressure variance was computed after

586 excluding stations at times when maximum precipitation exceeded 2 mm/hr. The green
587 lines indicate the four days during which 4.3 μm BT variance was highest.
588
589
590 Figure 11 shows the diurnal fluctuation in the variance of recorded pressure in the 2-6 hr
591 band in two regions of the study area. As shown in Figure 7a, gravity waves are most
592 frequently detected during the local night to the west of the Great Lakes during the
593 thunderstorm season (May through August). Most of the activity is concentrated from
594 38-44°N and 94-99°W. The mean pressure variance in this region, computed hourly, is
595 shown by the heavy black dotted curve in Figure 11. The mean rainfall in this area is
596 shown by the heavy blue dotted line. The lighter black dotted curve represents the mean
597 pressure variance in a region from 38-44°N and 84-89°W (i.e. a less active area located
598 10° to the east of the first). The mean rainfall for this area is shown by the lighter blue
599 dotted line. While the AIRS observations are made only twice per day, the TA
600 recordings are made continuously through the day. The two heavy vertical dashed lines
601 in Figure 11 at 01:30 and 13:30 LT represent the times of the AIRS observations. The
602 nighttime AIRS observation (at 01:30 LT) occurs at a time of high, but not quite
603 maximum, gravity wave activity on the ground. The daytime pass occurs nearly at the
604 time of minimum activity. Little activity is seen in the eastern region, as expected, and
605 any diurnal variations are weak.
606
607

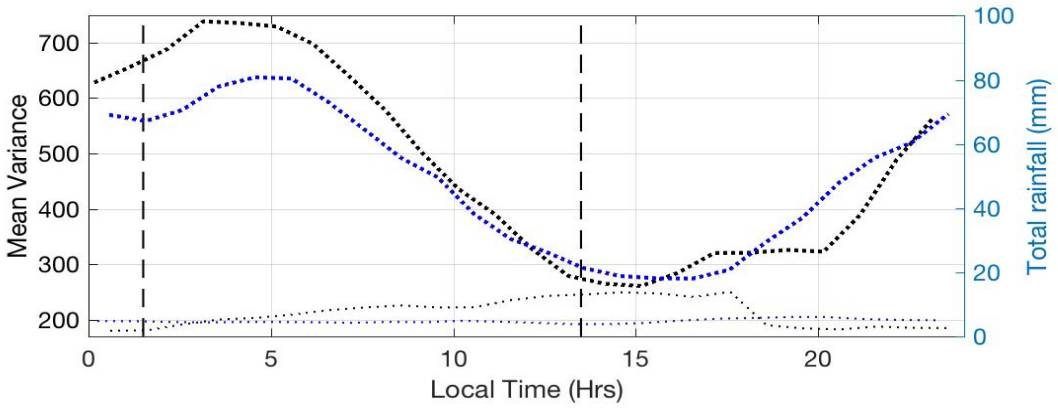

608
609
610 Figure 11. Mean TA pressure variance (Pa^2) and total rainfall per hour in two
611 rectangular regions near the Great Lakes. The heavy dashed curves represents
612 observations from 38-44°N and 94-99°W; black is the pressure variance, blue is the total
613 rainfall. The lighter dashed curve is from observations made in the same latitude range
614 but in the much less active area from 84-89°W, with black and blue lines representing the
615 pressure variance and total rainfall, respectively. The night and day AIRS overpass times
616 are represented by the vertical dashed lines.
617
618
619
620

6. Discussion and conclusions

Gravity wave detections made at the Earth's surface exhibit the same broad patterns as observed at stratospheric altitudes by the AIRS sensor (e.g. Figs. 7 and 9). However, we note that due to the movement of the TA over the duration of the study period, the western areas are sampled in earlier years than the eastern areas. It is possible that the lower level of AGW activity to the east reflects a decrease in AGW with time, rather than a spatial variation. Indeed, supplementary Figure S1 shows variations in gravity wave activity sensed by the AIRS instrument over the course of this 5-year study. The level of activity in the stratosphere to the west of the Great Lakes was relatively high in 2010, 2011 and in 2014. There was a lull in activity in 2012 and 2013. The decrease in activity in the stratosphere to the west of the Great Lakes that occurred between 2011 and 2012 is particularly striking, and important for this study given that the TA network was located in that area at that time. In addition, each station in the network was deployed for two years and therefore recorded data during two consecutive thunderstorm seasons. The supplementary Figure S2 shows a decrease in gravity wave activity detected by the TA from 2011 to 2012 - paralleling what is seen in the AIRS data. The 2012 data also indicate that despite the overall lower gravity wave occurrence rate, a decline in activity can still be observed from the western edge of the network (located where the gravity wave activity was concentrated in 2011) to the eastern edge of the network. The data suggest that the level of activity observed on the ground varied from year to year as it did in the stratosphere. We note that the region of highest gravity wave activity within the stratosphere is displaced slightly to the east of the corresponding region at ground level. The event shown in Figure 2a offers a possible explanation of this shift. The region where the 4.3 μm BT variances are greatest is located east of the convective source because of horizontal propagation of the waves and filtering effect of the background winds. This suggests that the gravity wave hotspot detected at ground level by the TA coincides with the convective source point of gravity waves observed by AIRS.

Seasonal and diurnal changes in gravity wave activity observed in the two datasets are also consistent. As seen in Figure 6, the level of activity on the ground varies seasonally (with a surge in activity during the thunderstorm season) as it does in the stratosphere (Hoffmann and Alexander, 2010). In Figure 7, the day/night differences at ground level also mirror those observed in the stratosphere (Figure 9). In summary, although the integrated results from 5 years of TA data cannot show in an absolute sense how gravity wave activity varied at ground-level spatially across the study area, they strongly suggest that it is only concentrated to the west of the Great Lakes and occurs mainly at nighttime during the thunderstorm season, similar to the AIRS results.

Expanding on the conclusions of the Stephan et al. (2016) case study, the agreement between the AIRS and TA datasets strongly suggests convection being the common origin between what is seen at ground level and in the stratosphere. The time series shown in Figure 10 permitted a quantitative assessment of the temporal linkage between gravity waves observed at ground level and both the level of gravity wave activity in the stratosphere and the convective activity observed by satellite, during the thunderstorm season in 2011. The correlation between gravity waves observed at the TA and

convective activity observed by AIRS is higher at night than during the day, but both are considered statistically significant. The 2-6 hr pressure variance at ground level, which is the proxy for gravity waves at ground level, was computed once every hour. With this sampling rate there is no discernable time lag between the two. Based on these observations, we conclude that gravity waves at the ground level are due to mesoscale convective systems. In previous studies (Hoffmann and Alexander, 2010; Grimsdell et al., 2010; Stefan and Alexander, 2015) it was established that the stratospheric gravity waves were also caused by convection. We conclude that convective activity to the west of the Great Lakes is the dominant source of gravity waves both at ground level and within the stratosphere. Day-to-day correlations between gravity waves in the stratosphere and at ground level are poorer, and only statistically significant at nighttime. Little gravity wave activity is detected in the stratosphere at times when the zonal winds are weak, as expected, since these waves are not expected to be detected by AIRS (Alexander and Barnet, 2007).

One other important difference between TA and AIRS datasets is that TA observations are sampled once per second while AIRS samples the region just twice per day. Any diurnal variations in gravity waves can therefore be examined in much greater detail at ground level - although as seen in Figure 11 the two AIRS passes are quite well timed to examine gravity wave occurrence near its peak and minimum. The TA data show that at ground-level in the smaller study area to the west of the Great Lakes there is a smooth, sinusoidal change in the frequency of gravity wave occurrence during the thunderstorm season each day. Comparison of this result with the corresponding result from the equal-sized region to the south of the Great lakes indicates that this diurnal trend is not ubiquitous. The diurnal change observed in this second area is relatively weak and does not reach its peak at night time.

Acknowledgements

This material is based upon work supported by the National Science Foundation under Grant Nos. EAR-1358520 and AGS-1519271. This study benefited greatly from services provided by the Array Network Facility (ANF) at UC San Diego and the Incorporated Research Institutions for Seismology (IRIS) Data Management Center (DMC). The barometric pressure data are available to the public at the Iris Data Management Center at http://ds.iris.edu/dms/. Funding for the atmospheric sensors in the TA was provided by NSF. AIRS data products are distributed by the NASA Goddard Earth Sciences Data Information and Services Center. ERA-Interim data were obtained from the European Centre for Medium-Range Weather Forecasts. Climate Prediction Center/National Centers for Environmental Prediction/National Weather Service/NOAA/U.S. Department of Commerce, and Joint Office for Science Support/University Corporation for Atmospheric Research, 2000: NCEP/CPC Four Kilometer Precipitation Set, Gauge and Radar. Research Data Archive at the National Center for Atmospheric Research, Computational and Information Systems Laboratory, Boulder, CO. [Available online at http://rda.ucar.edu/datasets/ds507.5/.] Accessed 26 Jul 2016.

References

Alexander, M. J., and C. Barnet, 2007: Using satellite observations to constrain parameterizations of gravity wave effects for global models, J. Atmos. Sci., 64, 1652-1665.

Alexander, M. J. and Pfister, L., 1995, Gravity wave momentum flux in the lower stratosphere over convection, Geophys. Res. Lett., 22, 2029–2032.

Alexander, M. J. and Rosenlof, K. H., 1996, Nonstationary gravity wave forcing of the stratospheric zonal mean wind, J. Geophys. Res., 101, 23465–23474.

Aumann, H. H., Chahine, M. T., Gautier, C., Goldberg, M. D., Kalnay, E., McMillin, L. M., Revercomb, H., Rosenkranz, P. W., Smith, W. L., Staelin, D. H., Strow, L. L., and Susskind, J., 2003, AIRS/AMSU/HSB on the Aqua Mission: Design, Science Objective, Data Products, and Processing Systems, IEEE T. Geosci. Remote Sens., 41, 253–264.

Bosart L. F. and J. P. Cussen, 1973: Gravity Wave Phenomena Accompanying East Coast Cyclogenesis. *Mon. Wea. Rev.*, 101, 446-454

Brunk, I. W., 1949: The Pressure Pulsation of 11 April 1944. *J. Meteorology*, 6, 395-401.

Busby, R.W., Vernon, F.L., Newman, R.L. & Astiz, L., 2006. Earth-Scope's USArray: advancing eastward, EOS, Trans. Am. Geophys. Un., 87(52), Fall Meet. Suppl., Abstract U41B-0820.

Cansi, Y., 1995. An automatic seismic event processing for detection and location: the P.M.C.C. method, Geophys. Res. Lett., 22, 1021–1024.

Carbone, R. E., and J. D. Tuttle, 2008, Rainfall Occurrence in the U.S. Warm Season: The Diurnal Cycle, J. Climate, 21, 4132-4146.

Chahine, M. T., Pagano, T. S., Aumann, H. H., Atlas, R., Barnet, C., Blaisdell, J., Chen, L., Divakarla, M., Fetzer, E. J., Goldberg, M., Gautier, C., Granger, S., Hannon, S., Irion, F. W., Kakar, R., Kalnay, E., Lambrigtsen, B. H., Lee, S., Marshall, J. L., McMillan, W. W., McMillin, L., Olsen, E. T., Revercomb, H., Rosenkranz, P., Smith,W. L., Staelin, D., Strow, L. L., Susskind,

J., Tobin, D., Wolf, W., and Zhou, L., 2006, AIRS: improving weather forecasting and providing new data on greenhouse gases, B. Am. Meteorol. Soc., 87, 911–926.

Choi, H. J., Chun, H. Y., Gong, J., and Wu, D. L., 2012, Comparison of gravity wave temperature variances from raybased spectral parameterization of convective gravity wave drag with AIRS observations, J. Geophys. Res., 117, D05115, doi:10.1029/2011JD016900.

de Groot-Hedlin, C.D., Hedlin, M.A.H. and Walker, K.T., 2014, Detection of gravity waves across the USArray: A case study, *Earth and Planetary Sciences Letters*, DOI: 10.1016/j.epsl.2013.06.042

de Groot-Hedlin, C.D. and Hedlin, M.A.H., 2015, A method for detecting and locating geophysical events using clusters of arrays, *Geophys. J. Int*., v203, 960-971, doi: 10.1093/gji/ggv345.

Eckermann, S. D., Wu, D. L., Doyle, J. D., Burris, J. F., McGee, T. J., Hostetler, C. A., Coy, L., Lawrence, B. N., Stephens, A., McCormack, J. P., and Hogan, T. F., 2006, Imaging gravity waves in lower stratospheric AMSU-A radiances, Part 2: Validation case study, Atmos. Chem. Phys., 6, 3343–3362, doi:10.5194/acp-6-3343-2006.

Eom, J. K., 1975: Analysis of the Internal Gravity Wave Occurrence of 19 April 1970 in the Midwest. *Mon. Wea. Rev.*, 103, 217-226

Gong, J., Wu, D. L., and Eckermann, S. D., 2012, Gravity wave variances and propagation derived from AIRS radiances, Atmos. Chem. Phys., 12, 1701–1720, doi:10.5194/acp-12-1701-2012.

Grimsdell, A. W., Alexander, M. J., May, P. T., and Hoffmann, L., 2010, Model study of waves generated by convection with direct validation via satellite, J. Atmos. Sci., 67, 1617–1631.

Havskov, J. & Ottemöller, L., 2010. Routine Data Processing in Earthquake Seismology, Springer.

Hoffmann, L. and Alexander, M.J., 2010, Occurrence frequency of convective gravity waves during the North American thunderstorm season, *Journal of Geophysical Research: Atmospheres*, v115, doi: 10.1029/2010JD014401.

Hoffmann, L., Xue, X. and M.J. Alexander, 2013, A global view of stratospheric gravity wave hotspots located with Atmospheric Infrared Sounder observations, *Journal of Geophysical Research: Atmospheres*, v118, 416-434, doi: 10.1029/2012JD018658.

Hoffmann, L., Alexander, M. J., Clerbaux, C., Grimsdell, A. W., Meyer, C. I., Rößler, T., and Tournier, B., 2014, Intercomparison of stratospheric gravity wave observations with AIRS and IASI, Atmos. Meas. Tech., 7, 4517–4537, doi:10.5194/amt-7-4517-2014.

Larsen, M. F., W. E. Swartz, and R. F. Woodman, 1982: Gravity-wave generation by thunderstorms observed with a vertically-pointing 430 MHZ radar. *Geophys. Res. Lett.,* 9, 571-574.

Mapes, B. J., 1993: Gregarious Tropical Convection. *J. Atmos. Sci*., 50, 2026-2037.

Pfister, L., Starr, W., Craig, R., Loewenstein, M., and Legg, M., 1986, Small-Scale Motions Observed by Aircraft in the Tropical Lower Stratosphere: Evidence for Mixing and its Relationship to Large-Scale Flows, J. Atmos. Sci., 43, 3210–3225.

Press, W. H., S. A. Teukolsky, W. T. Vetterling, and B. P. Flannery (2002), Numerical Recipes in C: The Art of Scientific Computing, vol. 1, 2nd ed., Cambridge Univ. Press.

Preusse, P., Eckermann, S. D., and Ern, M., 2008, Transparency of the atmosphere to short horizontal wavelength gravity waves, J. Geophys. Res., 113, D24104, doi:10.1029/2007JD009682.

Sato, K., C. Tsuchiya, M. J. Alexander, and L. Hoffmann, 2016: Climatology and Enso-related interannual variability of gravity waves in the Southern Hemisphere subtropical stratosphere revealed by high-resolution AIRS observations. *J. Geophys. Res. Atmos.*, 121, 7622—7640, doi: 10.1002/2015JD024462.

Scaife, A. A., Butchart, N., Warner, C. D., Stainforth, D., and Norton, W., 2000, Realistic quasi-biennial oscillations in a simulation of the global climate, Geophys. Res. Lett., 27, 3481–3484.

Stephan, C. C. and M. J. Alexander, 2015, Realistic simulations of atmospheric gravity waves over the continental U.S. using precipitation radar data. J. Adv. Model. Earth Syst.,07, doi:10.1002/2014MS000396.

Stephan, C.C., Alexander, M.J., Hedlin, M.A.H., de Groot-Hedlin, C.D. and Hoffmann, L., 2016, A case study on the far-field properties of propagating tropospheric gravity waves, *Monthly Weather Review*, v144, p2947-2961, DOI: 10.1175/MWR-D-16-0054.1.

Stobie, J. G., F. Einaudi and L. W. Uccellini, 1983: A Case Study of Gravity Waves—Convective Storms Interaction: 9 May 1979. *Mon. Wea. Rev.*, 40, 2804-2830.

Tepper, M., 1954: Pressure Jump Lines In Midwestern United States, January– August 1951. U.S. Weather Bureau Research Paper No. 37, 70 pp

Tsuchiya, C., K. Sato, M. J. Alexander, and L. Hoffmann, 2016: MJO-related intraseasonal variation of gravity waves in the Southern Hemisphere tropical stratosphere revealed by high-resolution AIRS observations. *J. Geophys. Res. Atmos.,* 121, 7641—7651, doi:10.1002/2015JD024463.

Tytell, J. Vernon, F., Hedlin, M.A.H., de Groot-Hedlin, C.D., Reyes, J., Busby, B., Hafner, K. and Eakins, J. 2015, The USArray Transportable Array as a Platform for Weather Observation and Research, *Bulletin of the American Meteorological Society*, http://dx.doi.org/10.1175/BAMS-D-14-00204.1.

Uccellini, L. W., 1975: A case study of apparent gravity wave initiation of severe convective storms. *Mon. Wea. Rev.*, 103, 497-513.

Wu, D. L., P. Preusse, S. D. Eckermann, J. H. Jiang, M. de la Torre Juarez, L. Coy, and D. Y. Wang, 2006: Remote sounding of atmospheric gravity waves with satellite limb and nadir techniques. *Adv. Space Res.*, 37, 2269-2277.

Yue, J., Thurairajah, B., Hoffmann, L., Alexander, M. J., Chandran, A., Taylor, M. J., Russell III, J. M., Randall, C. E., and Bailey, S. M., 2014, Concentric gravity waves in polar mesospheric clouds from the Cloud Imaging and Particle Size experiment, J. Geophys. Res., 119, 5115–5127, doi:10.1002/2013JD021385.